Identification of Brain Metastases Origins using Contrast Enhancement Patterns and Percentage Signal Recovery Values from Magnetic Resonance Imaging

Satvik Sharma[1], Rozy Gull[2], Kanika Kiran[3], Sabneet Sharma[4], Lalit Kumar Gupta[5]

[1,2,3,4]Assistant Professor, Department of Radiology, Rayat Bahara University, Kharar, Punjab 140103

[5]Professor, Department of Radiology, Rayat Bahara University, Kharar, Punjab 140103

ABSTRACT

Background: Brain metastases (BMs) are common in systemic malignancies and can affect patient prognosis significantly. The most prevalent diagnostic imaging modalities for characterising BMs, specifically contrast-enhanced CT and MRI, provide minimal insight into the biology of a lesion or its origin. Newer imaging modalities may benefit from DSC-MRI, and with imaging markers such as PSR, function to differentiate BMs, based on vascular physiology, and integrity of the blood-brain barrier (BBB). This study aimed to correlate PSR values and contrast enhancement patterns observed in DSC-MRI images to determine the primary origin of BMs, specifically differentiating between lung cancer and breast cancer.

Materials and Methods: A single-centre, retrospective study was conducted with 70 patients with confirmed BMs using DSC-MRI (48 lung and 22 breast carcinomas). Standard formulas were used to calculate PSR values. Enhancement patterns were classified as ring-shaped, heterogeneous, homogeneous, or cystic. The data were analysed descriptively, and receiver operating characteristic (ROC) curves were used with SPSS. Statistical significance was set to $p<0.05$.

Results: There was noted variation in PSR and enhancement patterns alone by tumour origin. Cystic and ring-shaped patterns were more prevalent in breast carcinoma, whereas heterogeneous patterns were observed more frequently in lung carcinoma. The overall mean PSR was 23.94% ± 9.26. From the ROC analysis, the area under the curve of PSR alone demonstrated weak discriminatory ability (AUC = 0.577, p = 0.303). Combining augmentation with enhancement pattern data increased diagnostic accuracy, most notably in the cystic patterns (AUC = 1.0, p = 0.034).

Discussion: The findings suggest that PSR and contrast enhancement may play a role in non-invasively suggesting the origin of tumour type in brain metastases. The PSR on its own may not be singularly sufficient; however, when combined with other forms of morphological imaging biomarkers, it does positively support enhancement in diagnostic confidence with tumour types with previously unknown malignancy sources.

Conclusion: PSR values obtained from DSC-MRI, coupled with patterns of contrast enhancement, suggest a plausible, non-invasive method for differentiating the primary origins of BMs. These findings warrant further investigation, including larger sample sizes and longitudinal studies, to validate these findings and systematically integrate the results from the diagnostic process into the priority order of routine clinical workflows.

Keywords: *Brain metastases, DSC-MRI, Percentage Signal Recovery (PSR), contrast enhancement, lung cancer, breast cancer.*

How to Cite: Satvik Sharma, Rozy Gull, Kanika Kiran, Sabneet Sharma, Lalit Kumar Gupta, (2025) Identification of Brain Metastases Origins using Contrast Enhancement Patterns and Percentage Signal Recovery Values from Magnetic Resonance Imaging, *Journal of Carcinogenesis, Vol.24, No.10s*, 611-620

1. INTRODUCTION

Brain metastases are severe complications that are common in systemic malignancies. The disease occurs when malignant cells are disseminated through the hematogenous route from the primary neoplasm to secondary malignant growth of the brain tissue (Achrol, et al., 2019). The diagnosis of brain metastases is complicated because they are the most prevalent adult intracranial neoplasm when compared to primary brain tumours (Arvanitis, Ferraro, & Jain, 2020). In all cancer patients, brain metastases are identified in approximately 10%-30 %, and there are important clinical implications for practice in oncology (Barnholtz-Sloan, et al., 2004). The primary tumours that produce the metastases will vary by type of cancer, but the most common cancers represented in the literature as related to brain metastases were overwhelmingly represented. Lung cancer is responsible for 40% - 50% of the metastatic lesions, Breast cancer is responsible for 15% - 25%, Melanoma and Renal cell

carcinoma are responsible for 5% - 20% and 5% - 10% respectively; and Colorectal Cancer has been reported to cause brain metastases in 4% - 6% of patients (Barajas, et al., 2010). Easily demonstrable increases in brain metastases have been seen over the last few years that are due to two important factors that affect patient prognoses: the development of new systemic therapies that include both the latest targeted therapies and

immunotherapies, and have afforded patients with greater longevity, and the development of sensitive high-resolution magnetic resonance imaging neuroimaging that can identify subtle and/or asymptomatic lesions (Berghoff, et al., 2016). It is essential to identify the source of the brain metastases, as each primary site imparts its unique clinical characteristics to the disease course and outcomes (Bisdas, et al., Perfusion CT in squamous cell carcinoma of the upper aerodigestive tract: Long-term predictive value of baseline perfusion CT measurements, 2011). The medical field has recognised that the original type of tumour drives their treatment decisions, since brain metastases in a patient with lung cancer will require very different medical treatment than for breast cancer brain metastases (Bisdas, et al., Perfusion CT in squamous cell carcinoma of the upper aerodigestive tract: A pilot study, 2011). Classic methods for identifying brain lesions, which are then used to identify primary lesions with contrast-enhanced computed tomography (CT) or magnetic resonance imaging (MRI), are inadequate because they do not provide biologic information or tissue of origin when there are no known primary lesions or multiple suspected malignancies (Cagney, et al., 2017). Dynamic susceptibility contrast (DSC) MRI is a sophisticated non-invasive imaging modality that is particularly employed in neuro-oncology (Essig, et al., 2013). DSC-MRI can help differentiate between brain metastases, and there are important differences that need to be highlighted (Franchino, Rudà, & Soffietti, 2018). DSC-MRI is significantly different from conventional MRI methods, which yield static images. With DSC-MRI, the information gained is functional, not structural, as the MRI scans acquired yield tumour perfusion data based on cerebral blood volume (CBV), blood flow, and vascular permeability (Hygino da Cruz, Rodriguez, Domingues, Gasparetto, & Sorensen, 2011). Breast cancer brain metastases routinely have higher PSR scores due to their vascular organisation and vascular structure, while lung cancers tend to have aggressive necrotic processes, which may be why the PSR scores are so low (Kang, et al., 2015). Recent studies have shown that perfusion messages differ significantly when comparing lesions, particularly with the use of PSR, creating an important diagnostic platform when the primary malignancy is unknown (Lee, Baird, Bell, Quarles, & Boxerman, 2019). Brain metastases most often occur in the cerebral hemispheres due to their readily available vascular supply (Lin & DeAngelis, 2015). Although the cerebellum and brainstem are less common locations for metastases, they are often associated with more severe neurological problems (Lockman, et al., 2010). The blood–brain barrier (BBB) is a crucial factor that influences the infiltration process of metastasis. Disruption of the BBB, mediated by tumour infiltration, is an important factor that enhances an imaging lesion on contrast (Serres, et al., 2014). The BBB provides a protective shield that preserves the brain's intact microenvironment while limiting the flow of chemical and biological assailants from the bloodstream into the brain (Shankar, et al., 2023). When metastases develop, the aspect of the BBB is disrupted, allowing MRI contrast agents to leak into the brain and produce specific enhancement characteristics (Soffietti, Ahluwalia, Lin, & Rudà, 2017). After the ability to extravasate across the BBB has been described in sufficient detail, some tumours can accomplish this action; however, there are large variations in this ability depending on the type of primary tumour (Suh, et al., 2020). These tumour-specific processes alter the way cancer cells interact, ultimately compromising the cerebral vasculature and neural stroma metabolically and thereby changing the structure, vascularity, and permeability of metastatic lesions in the brain (Tabouret, et al., 2012), (Wang, et al., 2021). Tumours that have established angiogenesis and immature vasculature, such as those that arise from lung or melanoma primaries, are more likely to have more irregular or hyperintense patterns of enhancement, compared to tumours that have relatively intact vascular channels, which are more likely to have lesser or more homogeneous enhancement (Yoo, et al., 2014), (Singh D. K., 2025). However, while MRI can characterise the shape and anatomy of lesions, it will usually be insufficient to provide the functional or physiological information required to characterise tumour behaviour and potential origin (Priti, 2025), (Singh S. M., 2025), (Ovais, 2025), (Ansari, 2023), (Jadon, 2025).

MATERIALS AND METHODS

Study Design: This single-centre retrospective observational study evaluated the percentage signal recovery (PSR) and contrast enhancement patterns in brain metastases to differentiate tissue characteristics and primary tumour origins (e.g., lung vs. breast cancer).

Study Setting: Data were exclusively retrieved from the FUJI PACS archive at Homi Bhabha Cancer Hospital and Research Centre, Mumbai, India. No prospective imaging or external site data collection occurred.

Study Population: Seventy patients with histologically confirmed brain metastases from primary tumours were included, covering a 48-month period from January 2023 to December 2026, to capture a variety of clinical presentations.

Sampling Criteria: Convenience sampling selected available cases strictly adhering to inclusion/exclusion criteria, prioritising diagnostic-quality DSC-MRI datasets.

Inclusion Criteria

- Patients of either sex with confirmed brain metastases diagnosed via contrast-enhanced MRI, specifically including delayed post-contrast T1-weighted (DSE-T1) sequences demonstrating distinct enhancement profiles.
- Histologically proven primary tumours with complete diagnostic DSC-MRI examinations assessing tumour perfusion, vascularity, and blood-brain barrier permeability.

Exclusion Criteria

- Missing, corrupted, or poor-quality imaging data (e.g., excessive artefacts).
- Incomplete clinical records or lack of histological confirmation.
- Metastases from unknown/non-primary tumours, post-surgical cases, or images without visible contrast enhancement.

Type of Tool and Image Acquisition Parameters: Imaging was performed on the Philips Ingenia 3T MRI system, which features a fully digital broadband architecture, dStream coil technology for coil-side digitisation (reducing noise), and compressed SENSE acceleration for faster scans with minimal motion artefacts. Key sequences included Dynamic Susceptibility Contrast (DSC)-MRI and Dynamic Contrast-Enhanced (DCE)-MRI for the quantitative evaluation of tumour vasculature and blood-brain barrier integrity.
DSC-MRI protocol used T2*-weighted single-shot echo-planar imaging (EPI):

- Repetition time (TR): 1500–2000 ms
- Echo time (TE): 30–40 ms
- Flip angle: 60–90°
- Field of view (FOV): Anatomy-dependent (typically 220–240 mm)
- Matrix size: 128 × 128
- Slice thickness: 4–5 mm (interslice gap 0–1 mm)
- Temporal resolution: 1–2 seconds per volume
- Number of dynamics: 50–80 (including 10–15 pre-contrast baseline volumes)
- Acquisition commenced seconds before intravenous gadolinium-based contrast agent (0.1 mmol/kg body weight, e.g., gadobutrol) injection at 3–5 mL/s via power injector, followed by saline flush; continued through first-pass, recirculation, and recovery phases.

Pre-contrast T1-weighted anatomical reference scans (e.g., 3D T1-MPRAGE) were acquired prior to the dynamic acquisition.

Methods of Data Collection: Retrospective datasets were extracted from FUJI PACS. Regions of interest (ROIs) were manually delineated on corresponding anatomical MRI slices within metastatic lesions, normal-appearing white matter, and necrotic areas. PSR was computed using:

$$\text{PSR} = \frac{S_1 - S_0}{S_m - S_0} \times 100$$

where S_0 = mean pre-contrast baseline signal intensity, S_m = minimum signal during contrast bolus passage, and S_1 = signal recovery plateau post-first-pass. Contrast enhancement patterns (heterogeneous, ring-like, cystic, homogeneous) were classified verbatim from original radiology reports.

Data Analysis: IBM SPSS Statistics (version unspecified; $p < 0.05$ significance threshold) performed all analyses. Descriptive statistics included means ± standard deviation (SD) for continuous PSR values and frequencies/percentages for categorical enhancement patterns and demographics. Between-group comparisons (e.g., PSR across patterns) used ANOVA or t-tests. Receiver Operating Characteristic (ROC) analysis assessed PSR phases (pre-contrast, minimum, recovery) for differentiating lung from breast cancer metastases, reporting area under the curve (AUC) with 95% confidence intervals (CI); AUC 0.5–0.7 (poor-fair), 0.7–0.9 (good), >0.9 (excellent) discrimination.

RESULTS

Descriptive statistical analysis to investigate differences in perfusion with PSR values and signal intensities across these patterns of enhancement revealed substantial differences in perfusion behaviour. The mean PSR value for all patients (N = 70) and all lesions was 23.94% ± 9.26, spanning a range of 8% to 46%. In ring lesions, PSR ranged from 11% to 46% with a mean PSR of 23.56% ± 9.91, and the signal intensities were markedly more heterogeneous. The signal intensity for the lesions had a mean baseline pre-contrast signal intensity of 1149.96, which decreased to a minimum of 826.70 upon passage of contrast and then returned to 1067.07 post-contrast. The heterogeneously enhancing lesions, most commonly found in the lung carcinoma group, had an average PSR

of 24.67% ± 9.17. The pre-contrast mean signal intensity was 1262.30, with the lowest exit signal intensity mean of 942.89 upon contrast transit, and it returned to an average of 1182.11. In this category, the signal intensity had the greatest range, indicating increased vascular heterogeneity, and possibly as a necrotic or haemorrhagic etiology. Cystic patterns of enhancement, which are more typical of metastatic breast cancer, had a mean PSR of 24.86% ± 8.25, slightly above the mean. These cystic lesions had a signal intensity of 1231.86, which dropped significantly upon passage to 879.14, then returned to 1133.57. An atypical subset, yet showed a homogeneous nature for PSR behaviour and therefore indicated homogeneous perfusion in the cystic tumorous spaces. Homogeneous enhancement patterns had the lowest mean PSR of 22.22% ± 9.46; however, the lesions were less heterogeneous in terms of signal intensity. The mean pre-contrast signal intensity of 1152.11 also showed a range, from a minimum of 778.00 to a maximum of 1069.00 post-contrast. The pattern was seen in both tumours, but without correlation. This detransformative analysis is summarised in Table 1.

Table 1 Demonstration of signal intensity and PSR along with each enhancement pattern

Descriptive Statistics				
Contrast_Enhance_Pat_rec		N	Mean	Std. Deviation
CYSTIC	PRE_SIG_CONT_BASE	7	1231.86	238.462
	MIN_SIG_DURING_CONT_PASS	7	879.14	451.043
	SIG_DURING_RECOVERY_PHASE	7	1133.57	279.236
	PSR_PCT	7	24.8571	8.25487
	Valid N (listwise)	7		
HETROGENOUS	PRE_SIG_CONT_BASE	27	1262.30	266.489
	MIN_SIG_DURING_CONT_PASS	27	942.89	350.371
	SIG_DURING_RECOVERY_PHASE	27	1182.11	276.039
	PSR_PCT	27	24.6667	9.16515
	Valid N (listwise)	27		
HOMOGENOUS	PRE_SIG_CONT_BASE	9	1152.11	132.590
	MIN_SIG_DURING_CONT_PASS	9	778.00	305.943
	SIG_DURING_RECOVERY_PHASE	9	1069.00	155.061
	PSR_PCT	9	22.2222	9.45751
	Valid N (listwise)	9		
RING SHAPED	PRE_SIG_CONT_BASE	27	1149.96	330.575
	MIN_SIG_DURING_CONT_PASS	27	826.70	378.972
	SIG_DURING_RECOVERY_PHASE	27	1067.07	329.264
	PSR_PCT	27	23.5556	9.91244
	Valid N (listwise)	27		
Overall	PRE_SIG_CONT_BASE	70	1201.76	278.959
	MIN_SIG_DURING_CONT_PASS	70	870.50	364.476
	SIG_DURING_RECOVERY_PHASE	70	1118.34	286.518
	PSR_PCT	70	23.9429	9.25780
	Valid N (listwise)	70		

Receiver operating characteristic curve (ROC) analysis of PSR values for differentiating CA breast from CA lung was performed, where the variable PSR shows a weak discriminatory ability with an AUC of 0.577; however, this difference is not statistically significant, p = 0.303.

ROC analysis of pre-signal contrast baseline for differentiating CA breast from CA lung in cystic contrast enhancement pattern. In which the variable PRE SIG CONT BASE shows great discriminatory ability with an AUC of 1.0, and this is statistically significant, p = 0.034. In a heterogeneous contrast enhancement pattern, the variable exhibits weak but discriminatory ability, with an AUC of 0.745, which is not statistically significant, although it is closer to the p value of 0.092, which is greater than the conventional threshold of 0.05. In a homogeneous contrast enhancement pattern, the variable exhibits weak discriminatory ability with an AUC of 0.611, which is not statistically significant (p = 0.606). In the ring contrast enhancement pattern, the variable demonstrates no discriminatory ability, with an AUC of 0.521, which lacks statistical significance, as indicated by a p-value of 0.86. The analysis for the pre-signal contrast baseline, used for differentiating CA lung from CA breast in cystic contrast enhancement, is shown in Table 2, along with the corresponding ROC curves in Figure 1.

Table 2 Demonstrating the overall cut point for the pre-signal contrast baseline for differentiating CA lung from CA breast.

subgroup	predictor	pos_class	direction	prevalence	optimal_cut point	AUC	sensitivity	specificity
Overall	PRE_SIG_CONT_BASE	CA BREAST	>=	0.314	1160	0.605	0.773	0.479
RING SHAPED	PRE_SIG_CONT_BASE	CA LUNG	>=	0.63	1450	0.521	0.294	0.9
CYSTIC	PRE_SIG_CONT_BASE	CA BREAST	>=	0.571	1180	1	1	1
HETROGENOUS	PRE_SIG_CONT_BASE	CA BREAST	>=	0.185	1545	0.745	0.6	0.955
HOMOGENOUS	PRE_SIG_CONT_BASE	CA BREAST	>=	0.333	1234	0.611	0.667	0.833

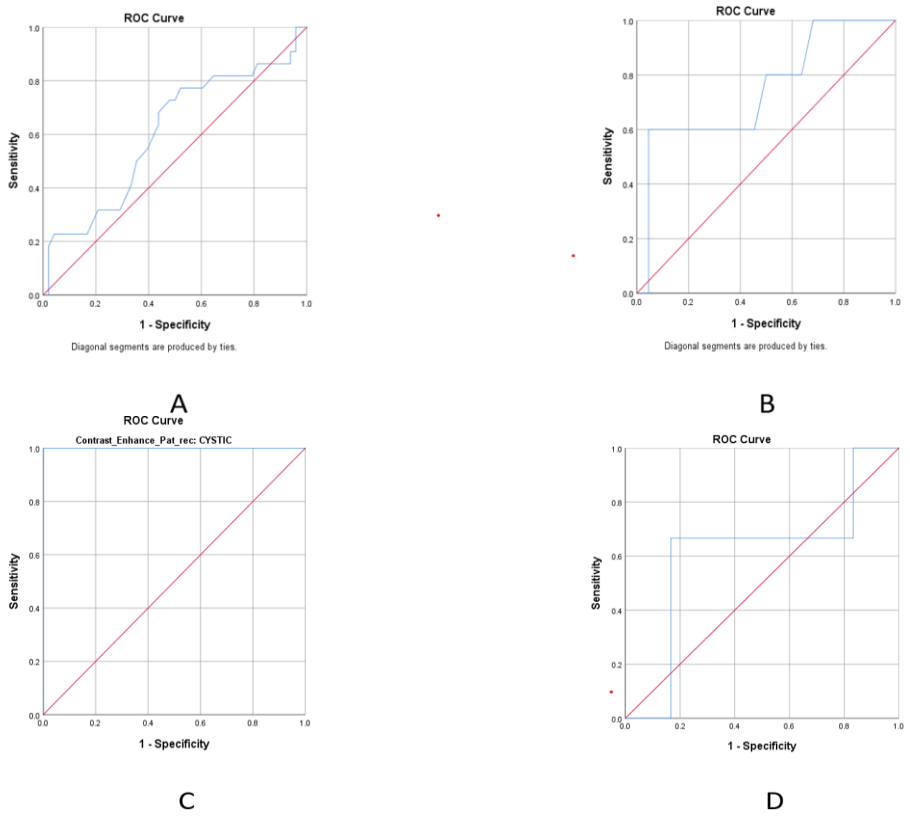

Figure 1. ROC curves for contrast enhancement patterns

A Ring (AUC = 0.521) B: Heterogeneous (AUC = 0.745)
C: Homogeneous (AUC = 0.611) D: Cystic (AUC = 1.0)

The overall cut point for the minimum signal during the contrast phase reveals that the cystic again demonstrates its overall discriminatory ability, with an AUC of 0.917, a specificity of 1.0, and a sensitivity of 0.75. Homogeneous and heterogeneous show moderate discriminatory ability with AUCs of 0.722 and 0.727, respectively. Homogeneous exhibits specificity of 1 and sensitivity of 0.5, while heterogeneous shows specificity of 0.864 and sensitivity of 0.6. The ring enhancement shows poor discriminatory ability, with an AUC of 0.603, specificity of 0-0.5, and sensitivity of 0.824. Overall, discriminatory ability is weak with an AUC of 0.528, and specificity of 0.958, and a sensitivity of 0.182. The overall cut point is shown in Table 3, and the associated ROC curves are shown in Figure 2.

subgroup	predictor	pos_class	direction	prevalence	optimal_cutpoint	AUC	sensitivity	specificity
Overall	MIN_SIG_DURING_CONT_PASS	CA BREAST	>=	0.314	1410	0.528	0.182	0.958
HOMOGENOUS	MIN_SIG_DURING_CONT_PASS	CA LUNG	>=	0.667	1030	0.722	0.5	1
RING SHAPED	MIN_SIG_DURING_CONT_PASS	CA LUNG	>=	0.63	580	0.603	0.824	0.5
CYSTIC	MIN_SIG_DURING_CONT_PASS	CA BREAST	>=	0.571	1160	0.917	0.75	1
HETROGENOUS	MIN_SIG_DURING_CONT_PASS	CA BREAST	>=	0.185	1200	0.727	0.6	0.864

Table 3 Shows the optimum cut point values for minimum signal during the contrast phase.

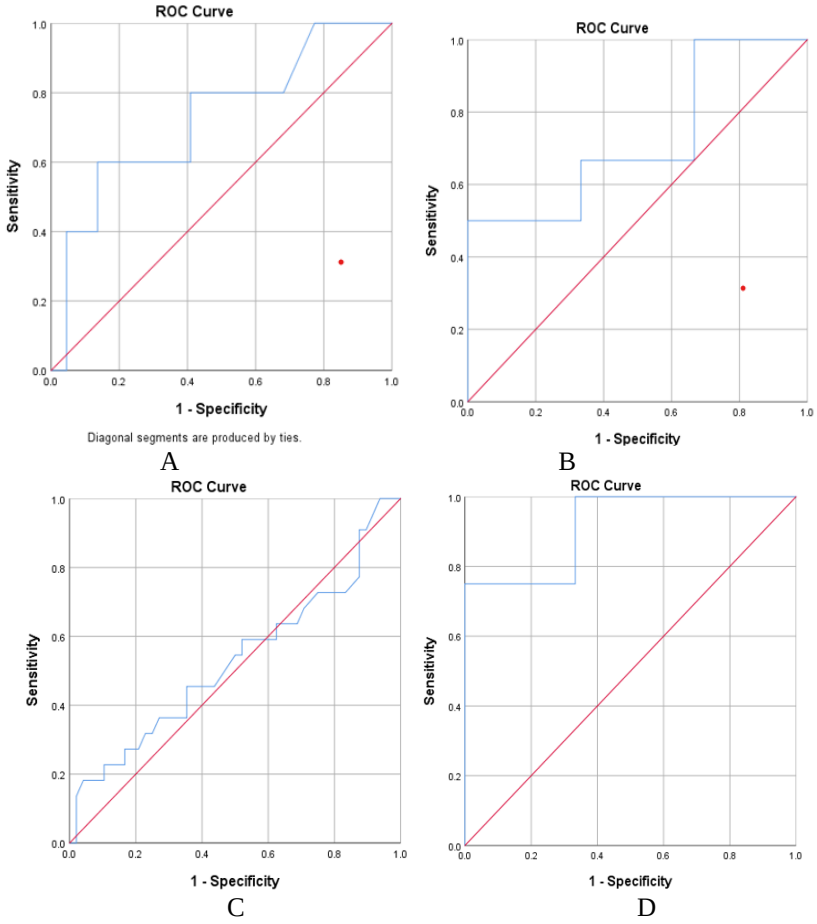

Figure 2. ROC curves for the minimum signal during contrast passage

***A**: Ring (AUC = 0.603) **B**: Heterogeneous (AUC = 0.727) **C**: Homogeneous (AUC = 0.722) **D**: Cystic (AUC = 0.917)*

Overall, the cut point for the signal during the recovery phase is as follows: cystic has the best discriminatory ability with an AUC of 1.0 and specificity and sensitivity of 1.0, while heterogeneous has moderate discriminatory ability with an AUC of 0.759, specificity of 0.955, and sensitivity of 0.6. Both ring and homogeneous showed poor discriminatory ability, with AUCs of 0.53 and 0.61, specificities of 0.9 and 0.667, and sensitivities of 0.294 and 0.833. Overall discriminatory ability is weak with an AUC of 0.314, a specificity of 0.604, and a sensitivity of 0.591. The optimal cut points for the signal during the recovery phase, as shown in Table 4, and the corresponding ROC curves are presented in Figure 3.

Table 4 Shows the minimum cut point values for the recovery phase.

subgroup	predictor	pos_class	direction	prevalence	optimal_cut point	AUC	sensitivity	specificity
Overall	SIG_DURING_RECOVERY_PHASE	CA BREAST	>=	0.314	1176	0.581	0.591	0.604
HOMOGENOUS	SIG_DURING_RECOVERY_PHASE	CA LUNG	>=	0.667	1020	0.611	0.833	0.667
RING SHAPED	SIG_DURING_RECOVERY_PHASE	CA LUNG	>=	0.63	1330	0.532	0.294	0.9
CYSTIC	SIG_DURING_RECOVERY_PHASE	CA BREAST	>=	0.571	1050	1	1	1
HETROGENOUS	SIG_DURING_RECOVERY_PHASE	CA BREAST	>=	0.185	1525	0.759	0.6	0.955

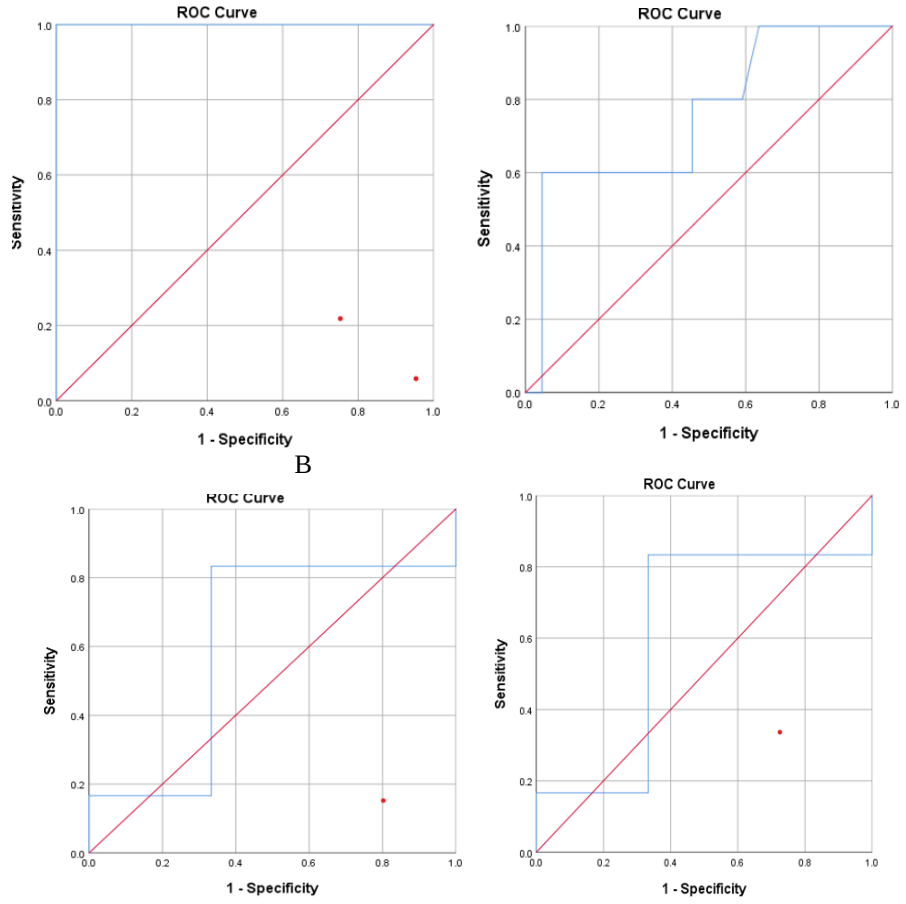

***Figure 3. ROC curves for signal during recovery phase A**: Ring (AUC = 0.532), **B**: Heterogeneous (AUC = 0.759) **C**: Homogeneous (AUC = 0.611) **D**: Cystic (AUC = 1.0)*

DISCUSSION

This investigation evaluated the role of patterns of contrast enhancement and Percentage Signal Recovery (PSR) on DSC-MRI to differentiate brain metastases that originated from lung and breast cancers.

The study population consisted of 70 patients, including 48 with lung cancer and 22 with breast cancer. PSR and patterns of contrast enhancement are assessed in combination. Concerning features of contrast enhancement, ring and heterogeneous patterns were the most common, while cystic shapes and homogeneous patterns were the least common. PSR values were also assessed for each pattern and compared between lung metastases and breast metastases. The findings suggest that

certain patterns of enhancement, such as cystic and heterogeneous, along with PSR values, can be used to discriminate between metastatic origins. Breast cancer metastases were associated with more cystic enhancement and had higher PSR values. Lung carcinoma metastases demonstrated several heterogeneous patterns and a lower propensity for higher PSR values. These findings align with the base study by Shankar et al. (2023), which indicates that PSR values vary according to tumour type, as well as suggesting that PSR values reflect the vascular and structural features of lesions [17].

In a separate study by Lee et al. (2019), the authors note that PSR has significant utility in distinguishing primary central nervous system lymphomas from other tumour types, comparing PSR with preradiotherapy baseline signal intensity, which together provides a better diagnostic tool for differentiation purposes [18]. This study does not explicitly differentiate between metastases from the breast and those from the lung. However, the authors' points about rCBV, DSC-MRI protocols, and the utility of consistent imaging parameters are important points that relate to this study, as the ability to reliably measure PSR values depends on imaging parameters remaining consistent.

The study by Surendra et al. (2020) also provides support for our findings, as it suggests that PSR performed better or at least as planned when compared to rCBV in differentiating common brain neoplasms [19]. Still, their findings relate increased PSR to lesions with more complete blood-brain barrier disruption, which is consistent with our findings of cystic metastases being more prevalent in breast cancer having higher PSR values.

One of the greatest strengths of this study is the simultaneous review of both PSR and enhancement pattern concurrently as imaging markers, which provided a wealth of detail in the findings regarding the metastatic origins of neoplasms in the brain. The ROC analysis also confirmed that cystic enhancement, especially with breast cancer metastases, was very discriminative. Additionally, the incorporation of restraint from PSR into the combined analysis provided confidence in these results.

The study does have limitations, such as a retrospective design and the discrepancies from irregular subjects between lung and breast cancer, with a larger number of cases of lung cancer. In addition, the influence of motion artefact, variation in imaging parameters, and lesion heterogeneity can impact PSR values. Another limitation of this study is that there were no other perfusion biomarkers, rCBV or Ktrans, to contribute to a meaningful discussion on the differentiation aspect of the study. From a clinical perspective, the findings suggest that combining both enhancement patterns and PSR values could help radiologists and oncologists better understand the primary origin of brain metastases and potentially reduce the differential, thereby guiding treatment more precisely.

The findings from this information suggest a useful application in clinical scenarios where the primary malignancy is unknown. A brain lesion that displays a cystic enhancement pattern and has a high PSR may favour breast carcinoma origin and might assist in expediting imaging or biopsy workup. Heterogeneous patterns with low PSR may suggest lung origin. If imaging knowledge could assist oncologists in the early stages of making diagnostic decisions and distinguishing between conditions more quickly and non-invasively, methods or targeted treatment approaches may be considered useful. Particularly at the time when there was no evidence of systemic disease or when tissue sampling posed a danger.

Future studies should include multi-centre studies, similarly balanced cohorts, and, in addition, suggest offering more imaging biomarkers to legitimise the overall diagnostic value.

Limitations

The limitations of the study may be attributed to its retrospective nature and the relatively small cohort. Additionally, limiting the scope to only two primary cancers has limited generalizability to other primary cancers. The study should have included other variables, such as rCBV and rCBF, that may contribute to increasing diagnostic accuracy. There was no longitudinal follow-up; therefore, we were unable to gather additional information regarding temporal changes in the PSR values over time, or whether these changes were related to treatment response or disease progression.

CONCLUSION

In conclusion, this study demonstrated the ability to differentiate the primary source of brain metastases from breast and lung carcinomas based on the differing contrast enhancement patterns observed on DSC MRI and the PSR values. Importantly, while the PSR had limited diagnostic capabilities in and of itself, it performed significantly better when interpreting the morphological characteristics of the contrast enhancement patterns in conjunction with the PSR. For example, cystic and heterogeneous enhancement could separate CA lung from CA breast, but had a lower degree of accuracy. Additionally, while homogeneous enhancement and ring enhancement were able to moderately and weakly classify, respectively, no level of accuracy was able to convey primary sources.

Future studies would need to reproduce these preliminary results in longitudinal, multicentre, and prospective cohorts. In

addition, compiling additional advanced imaging biomarkers and/or machine learning for pattern recognition and relationship to molecular tumour profiles would help improve diagnostic accuracy. The incorporation of these methods could assist us in personalising treatment plans and provide earlier and more accurate diagnoses by reducing the need for invasive options, resulting in more effective therapeutics and options for patients with brain metastases.

REFRENCES

1. Achrol, A. S., Rennert, R. C., Anders, C., Soffietti, R., Ahluwalia, M. S., & Nayak, L. (2019). Brain metastases. *Nature Reviews Disease Primers*, 5.
2. Ansari, M. I. (2023). A cross-sectional survey on insight into the current perceptions of Indian radiologists, radiographers, radiology trainees, and medical imaging students on the future impact of artificial intelligence (AI) on the profession. *Journal of Pharmaceutical Negative Results*, 1686–1699.
3. Arvanitis, C. D., Ferraro, G. B., & Jain, R. K. (2020). The blood–brain barrier and blood–tumour barrier in brain tumours and metastases. *Nature Reviews Cancer*, 26–41.
4. Barajas, R. F., Chang, J. S., Sneed, P. K., Segal, M. R., McDermott, M. W., & Cha, S. (2010). Distinguishing recurrent intra-axial metastatic tumor from radiation necrosis following gamma knife radiosurgery using DSC perfusion MRI. *AJNR American Journal of Neuroradiology*, 62–268.
5. Barnholtz-Sloan, J. S., Sloan, A. E., Davis, F. G., Vigneau, F. D., Lai, P., & Sawaya, R. E. (2004). Incidence proportions of brain metastases in patients diagnosed (1973–2001) in the Metropolitan Detroit Cancer Surveillance System. *Journal of Clinical Oncology*, 2865–2872.
6. Berghoff, A. S., Preusser, M., Schur, S., Höller, C., Streubel, B., & Hackl, M. (2016). Correlation of immune phenotype with IDH mutation in brain metastases. *Neuro-Oncology*, 258–265.
7. Bisdas, S., Rumboldt, Z., Surlan-Popovic, K., Aquilina, K., Blythe, J. S., & Shen, P. Y. (2011). Perfusion CT in squamous cell carcinoma of the upper aerodigestive tract: A pilot study. *European Radiology*, 885–892.
8. Bisdas, S., Rumboldt, Z., Surlan-Popovic, K., Baghi, M., Koh, T. S., & Vogl, T. J. (2011). Perfusion CT in squamous cell carcinoma of the upper aerodigestive tract: Long-term predictive value of baseline perfusion CT measurements. *AJNR American Journal of Neuroradiology*, 576–581.
9. Cagney, D. N., Martin, A. M., Catalano, P. J., Redig, A. J., Lin, N. U., & Lee, E. Q. (2017). Incidence and prognosis of patients with brain metastases at diagnosis of systemic malignancy. *Neuro-Oncology*, 1511–1521.
10. Essig, M., Shiroishi, M. S., Nguyen, T. B., Saake, M., Provenzale, J. M., & Enterline, D. (2013). Perfusion MRI: The five most frequently asked technical questions. *AJR American Journal of Roentgenology*, 24–34.
11. Franchino, F., Rudà, R., & Soffietti, R. (2018). Mechanisms and therapy for cancer metastasis to the brain. *Frontiers in Oncology*, 161.
12. Hygino da Cruz, L. C., Rodriguez, I., Domingues, R. C., Gasparetto, E. L., & Sorensen, A. G. (2011). Pseudoprogression and pseudoresponse: Imaging challenges in posttreatment glioma. *AJNR American Journal of Neuroradiology*, 1978–1985.
13. Jadon, M. S. (2025). Diagnostic concordance of self-collected versus technician-collected swabs for SARS-CoV-2 detection. *Journal of Applied Bioanalysis*, 257–267.
14. Kang, Y., Choi, S. H., Kim, Y. J., Kim, K. G., Sohn, C. H., & Kim, J. H. (2015). Gliomas: Histogram analysis of ADC maps with standard- or high-b-value diffusion-weighted MR imaging. *Radiology*, 876–886.
15. Lee, M. D., Baird, G. L., Bell, L. C., Quarles, C. C., & Boxerman, J. L. (2019). Utility of percentage signal recovery and baseline signal in DSC-MRI optimized for rCBV measurement. *AJNR American Journal of Neuroradiology*, 1445–1450.
16. Lin, X., & DeAngelis, L. M. (2015). Treatment of brain metastases. *Journal of Clinical Oncology*, 3475–3484.
17. Lockman, P. R., Mittapalli, R. K., Taskar, K. S., Rudraraju, V., Gril, B., & Bohn, K. A. (2010). Heterogeneous blood–tumor barrier permeability determines drug efficacy in experimental brain metastases. *Clinical Cancer Research*, 5664–5678.
18. Ovais, R. G. (2025). Addressing communication difficulties in MRI: Radiographers' approaches for deaf and hard-of-hearing patients. *International Journal of Environmental Sciences*, 1677–1687.
19. Priti, K. K. (2025). Diagnostic and prognostic role of chest CT in oncologic patients with COVID-19 pneumonia: An Indian perspective. *International Journal of Environmental Sciences*, 4152–4159.
20. Serres, S., Soto, M. S., Hamilton, A., McAteer, M. A., Carbonell, W. S., & Robson, M. D. (2014). Molecular MRI enables early and sensitive detection of brain metastases. *Proceedings of the National Academy of Sciences*, 2299–2304.
21. Shankar, A., Brar, R., Dwivedi, A., Rathore, D. S., Prasad, A., & Rana, S. (2023). Utility of percentage signal recovery derived from DSC perfusion MRI. *Journal of Clinical and Scientific Research*, 242–247.
22. Singh, D. K. (2025). Artificial intelligence in predictive oncology: A clinical study using machine learning for cancer detection. *Journal of Carcinogenesis*, 228-240.
23. Singh, S. M. (2025). Population-based assessment of female thoracic dimensions and body habitus via CT imaging. *International Journal of Environmental Sciences*, 60–68.

24. Soffietti, R., Ahluwalia, M., Lin, N., & Rudà, R. (2017). Management of brain metastases according to molecular subtypes. *Nature Reviews Neurology*, 709–720.
25. Suh, J. H., Kotecha, R., Chao, S. T., Ahluwalia, M. S., Sahgal, A., & Chang, E. L. (2020). Current approaches to the management of brain metastases. *Nature Reviews Clinical Oncology*, 279–299.
26. Tabouret, E., Chinot, O., Metellus, P., Tallet, A., Viens, P., & Gonçalves, A. (2012). Recent trends in epidemiology of brain metastases. *Anticancer Research*, 4655–4662.
27. Wang, Y., Xia, W., Liu, B., Zhou, L., Ni, M., & Zhang, R. (2021). Spatial distribution of brain metastasis from small cell lung cancer. *Cancer Imaging*, 1–10.
28. Yoo, H., Kim, Y. Z., Nam, B. H., Shin, S. H., Yang, H. S., & Lee, J. S. (2014). Reduced local recurrence through microscopic total resection. *Journal of Neurosurgery*, 295–303.